Gas-Liquid Flow Regime Maps for Horizontal Pipelines: Predicting Flow Regimes Using Dimensionless Parameter Groups

Olusegun Samson Osundare [1,*], Alexander Elliott [1], Gioia Falcone [1], Liyun Lao [2]**

[1] James Watt School of Engineering, University of Glasgow, Glasgow, G12 8QQ, United Kingdom; o.osundare.1@research.gla.ac.uk; alex.j.elliott@cranfield.ac.uk; Gioia.Falcone@glasgow.ac.uk;
[2] Centre for Thermal Energy Systems and Materials, Cranfield University, MK43 0AL, United Kingdom; l.lao@cranfield.ac.uk
* Correspondence: o.osundare.1@research.gla.ac.uk; Tel.: +447466878853 (O.S.O.)
** Now with Cranfield University

ABSTRACT

Flow regime maps are essential to gas-liquid flow applications in many industrial processes to accurately identify the flow regimes before estimating multiphase features. Flow regime classifications were originally based on visual observations of two-phase flow experiments. The observations were mapped on two-dimensional plots (called "flow regime maps") and the boundaries between regimes determined. Over the years, different coordinates have been proposed for the maps (e.g., superficial velocities and momentum fluxes), in search for parameters that are independent of the given experimental set-up. This paper reports a study on developing new flow regime maps with a broader range of applications by using dimensionless parameter groups as the map coordinates. Various flow regime maps were developed with the use of different combinations of these parameter groups, then they were examined and assessed using datasets from published experimental research and the MultiFlowMet II project for validation. This initial feasibility study develops proof-of-concept flow regime maps that demonstrate the potential of dimensionless parameter groups to more accurately characterise multiphase flow in horizontal pipes, with the optimisation of these maps being considered in future works. The analysis revealed that combinations of the mixture Froude number (Fr_m) versus the ratio of gas superficial velocity to liquid superficial velocity (v_{SG}/v_{SL}), with the liquid phase Froude number (Fr_L) versus the gas phase Froude number (Fr_G) show potential for unambiguous identification and mapping of flow regimes, even for datasets with a wider range of operating conditions.

Keywords: Air-water; flow pattern; dimensionless parameters; transition boundary; two-phase flow; Froude number.

1 INTRODUCTION

Two-phase flows are found in many industrial processes, such as oil and gas production wells and pipelines, heat-exchangers, chemical engineering process plants, nuclear reactors, boiler systems, power plants, geothermal energy, and refrigeration (Humami et al., 2018). In these industries, the predictions of flow characteristics such as pressure-drop and phase fractions are of interest, which are strongly dependent on the prevailing flow regime in the pipes. Therefore, the first step in predicting two-phase flow characteristics is to determine the flow regime (Lips and Meyer, 2011). Different flow regimes can be related to different fluid dynamic mechanisms, so distinct models and correlations could apply only to a specific flow regime (Lips and Meyer, 2011). Flow rates, phases properties, and pipe geometrical characteristics (i.e. equivalent diameter, pipe orientation and roughness) are factors that dictate the occurrence of a particular flow regime (Tzotzi et al., 2011). The community accepts that flow regimes of gas-liquid horizontal flow can be classified as stratified-smooth flow, stratified-wavy flow, slug flow, elongated bubble flow (or plug flow), bubbly flow, disperse bubble flow, annular flow, and wispy annular flow (Amaya-Gomez et al., 2019; França and Lahey, 1992; Zhang et al., 2004). These flow regimes are defined by visual observations mainly, which are subjective (Lin and Hanratty, 1987) and the transition from one flow regime to another identified by various observers can differ.

Some discrepancies are observed when data from different sources are brought together and might be due to differences in terminology used by various investigators/authors when the data were collected. Vásquez et al. (2012) categorised bubble flow as dispersed flow, while Govier & Omer (1962) gave bubble flow a distinct class. Usually, transition always exists between two different but neighbouring flow regimes (Kokal and Stanislav, 1989), except for the transition of stratified flow to intermittent flow at low gas velocities (Tzotzi et al., 2011). Shoham (1982) identified a flow configuration as wavy annular flow, which is a subclass of annular flow, while the same flow configuration was considered by Mandhane et al. (1974) as slug flow. Mandhane et al. (1974) grouped bubble flow and plug flow together, as shown in Figure 1 and only separated dispersed bubble flow when the bubbles were uniformly distributed in the liquid phase. Shoham (1982) did not mention bubble flow in his flow regimes classification, but recognised dispersed bubble flow once the elongated bubbles break down into small bubbles. Some researchers only consider a flow configuration to be dispersed bubble flow after the small bubbles have been distributed across the entire pipe (Coleman and Garimella, 1999; Mandhane et al., 1974).

Due to the challenges outlined in the previous paragraph, no universally accepted flow regime map for gas-liquid flow in the horizontal pipeline has been established (Baba et al., 2019; Saha, 2015). Most developed flow regime maps are dimensional, and only applicable to the experimental datasets used for constructing them (Anumbe, 2018; Brennen, 2005; Cheng et al., 2008). A flow regime map based on dimensionless parameter coordinates would have a broader range of application as the parameters are expected to normalise and delineate all the data points with similar flow characteristics into an area on the map.

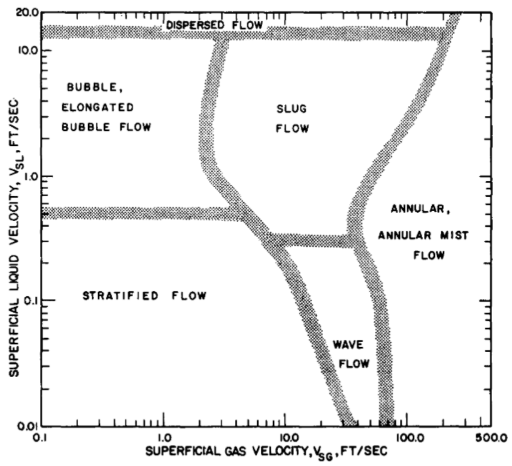

Figure 1: Gas-liquid flow regime map in horizontal pipe (Mandhane *et al.,* 1974).

A popular approach in dimensionless analysis is the Buckingham Π theorem, where a physical process that satisfies dimensional homogeneity principle and has n relevant variables and m independent dimensions, can be reduced to a relationship between n and m dimensionless parameters (Farokhpoor et al., 2020). However, there is limited success in applying dimensional analysis to gas-liquid flow because it results in many dimensionless parameters and infinite ways in which they can be combined to produce equally valid dimensionless parameter groups (Farokhpoor et al., 2020; Shoham, 2005).

Dimensionless parameter groups are formed by incorporating the forces acting on the gas-liquid flow which include inertia, viscousity, gravity (buoyancy) and surface tension (capillary) (Bai and Bai, 2019; Osundare et al., 2020; Zhao and Rezkallah, 1993). The co-current flow of gas and liquid in a horizontal pipe may result in different flow regimes due to various forces acting on the mixture. The balance between these forces dictates the dominating flow regime.

At low fluid velocities, the gravity force dominates and generates a tendency for stratification in the vertical direction, i.e. the liquid phase flows at the bottom part of the pipe while the gas phase flows at the top of the pipe. The surface tension force tends to wick the liquid phase around the pipe circumference, thereby creating annular flow; it also tends to form strong interfacial forces that can lead to slug flow (Shi et al., 2017). At high velocity, the inertia force tends to manifest in turbulent fluctuations, where dispersed flows occur. The viscous force promotes annular flow. Therefore, various flow regimes are formed due to the interaction between several forces on the flow components(Bai and Bai, 2019).

Various combinations of coordinates for presenting flow regime maps in a 2D graph have been considered in the literature; a chronological overview of developments for generating regime maps for gas-liquid flow in horizontal pipelines is presented in Appendix A. Superficial liquid velocity (v_{SL}) versus superficial gas velocity (v_{SG}) is the most frequently used for constructing flow maps in recent times. This may be due to the assumption that transition curves are least sensitive to changes in pipe diameter and fluid properties when superficial liquid velocity (v_{SL}) and superficial gas velocity (v_{SG}) are used as coordinates (Lin and Hanratty, 1987). Al-Sheikh et al. (1970) and Mandhane et al. (1974) developed flow regime map based on the AGA-API data bank, which allowed using a wide range of values for flow parameters and physical properties of gas and liquid in their studies. Some researchers developed their flow regime maps based on data from other studies (Baker, 1954; Jayawardena et al., 1997; Spedding and Nguyen, 1980).

Various names are given to the observed flow regimes, and different classifications of flow regimes have been used by many of the researchers. Wong and Yau (1997) and Spedding and Chen (1980) identified 16 and 13 distinguishable flow regimes, respectively. However, all the flow regimes can be grouped in 4 broader classes of stratified, intermittent, annular, and dispersed bubble flow. Some other researchers prefer to work with 6 groups by splitting stratified flow into stratified-smooth and stratified-wavy, and the intermittent flow into plug and slug flow.

The clear disparities between existing, dimensional flow regime maps necessitate a new, more transferable approach. In this paper, the authors propose the use of dimensionless parameter groups to develop flow regime maps that are consistent across different flow loops. Section 2 outlines the methodology for defining these initial proof-of-concept maps. In Section 3, the resulting maps are presented and validated using data from the MultiFlowMet II project (Elliott et al., 2021). Conclusions and recommendations for multiphase flow practitioners are presented in Section 4.

2 METHODOLOGY

In this project, two categories of datasets were employed for analysis, those extracted from experimental works in the literature and those from the MultiFlowMet II project.

The dimensional analysis does not account for heat transfer effects, as they do not strongly influence hydrodynamics in long-distance transportation of oil and gas (Farokhpoor et al., 2020). There are nine relevant independent variables for a fully developed, steady-state, isothermal gas-liquid flow in a horizontal pipeline. These include superficial gas and liquid velocities (v_{SG}) and (v_{SL}), gas and liquid densities (ρ_G), and (ρ_L), pipe diameter (d), gas and liquid viscosities (μ_G) and (μ_L), surface tension (σ), , and the acceleration due to gravity (g).The three fundamental dimensions are mass (M), length (L) and time (T). Based on the Buckingham Π theorem, the number of system variables minus the number of fundamental variables is equal to the number of dimensionless groups. Hence, the horizontal gas-liquid flow system will have eight dimensionless parameter groups, which are (i) density ratio, (ii) square of gas-phase Froude number, (iii) ratio of superficial liquid velocity to superficial gas velocity, (iv) inverse of gas-phase Reynolds number, (v) inverse of liquid phase Reynolds number, and (vi) inverse of gas-phase Weber number.

2.1.1 Formation of the dimensionless parameter groups

Dimensionless numbers are ratios of any two of the forces (inertia, viscous, gravity and surface tension) acting on a flow system. However, to know the influence of more than two forces, selected dimensionless numbers (resulting from dimensional analysis performed on two-phase horizontal flow) were combined in various ways to form dimensionless parameter groups. The target was to combine as many as possible forces in a dimensionless parameter group but avoid having forces in exponential form, as it may be unphysical to interpret exponential force in a flow system. Among the relevant dimensionless parameter groups identified in this project are:

i. The ratio of Reynolds number to Eötvös number (Re/Eo), which combines all the forces acting on the flow system. A high value of Re/Eo would favour a flow system where inertia and surface tension forces prevail.
ii. The Froude number (Fr) captures the ratio of inertia to gravity forces.
iii. The ratio of gravity force to viscous force (G/V), which is derived by dividing the Reynolds number by the square of the Froude number, so that the inertia force cancels out. At a high G/V value, gravity force prevails.
iv. The capillary number (Ca) is the ratio of viscous to surface tension forces.

Various combinations of these dimensionless parameter groups governing the gas-liquid flow are formed by the ratio of various forces acting on the flow. The ratio of inertia force to viscous, gravity and surface tension forces are Reynolds number, Froude number and Weber number, respectively. Another valuable dimensionless parameter is the Eötvös number, which is the ratio of gravity force to surface tension force. The ratio of gravity force (G) to viscous force (V) is not captured in any of the dimensionless numbers, and hence it is estimated as suggested by Shi and Yeung (2017). The G/V can also be expressed as the ratio of Reynolds number (Re) to square of Froude number (Fr^2). Equations 1 to 5 present relevant dimensionless parameter groups, where forces influencing gas-liquid flow are captured.

$$\frac{Re_i}{Eo} = \frac{\rho_i v_{si}}{\mu_i}\frac{\sigma}{\Delta\rho g d} \tag{1}$$

$$Fr_i^2 = \frac{v_i^2}{gd}\frac{\rho_i}{\Delta\rho} \tag{2}$$

$$\frac{G}{V} = \frac{\Delta\rho g d^2}{\mu_i \, v_i} \qquad 3$$

$$Ca_i = \frac{\mu_i v_i}{\sigma} \qquad 4$$

The relevant dimensionless parameter groups Re/Eo, Fr, G/V and Ca stand for the ratio of Reynolds number to Eötvös number, Froude number, the ratio of gravity to viscous force, and capillary number, respectively. Note: where, i stands for subscripts $_m$, $_G$ and $_L$ that is mixture component, gas-phase, and liquid-phase, respectively. The symbols ρ, Δρ, v, d, σ, g, Q and μ denote density, density difference, velocity, pipe diameter, surface tension, acceleration due to gravity, volumetric flow rate and viscosity, respectively. The v_{SG} and v_{SL} are superficial gas velocity and superficial liquid velocity, respectively.

The volume average method was employed to estimate the mixture density and viscosity, as shown in Equations 6 and 7. At the same time, the mixture velocity was estimated as the sum of the superficial velocity of both phases.

$$\rho_m = \rho_L \lambda + \rho_G (1 - \lambda), \qquad 5$$

$$\mu_m = \mu_L \lambda + \mu_G (1 - \lambda), \qquad 6$$

where λ is the volume of liquid fraction, calculated as

$$\lambda = \frac{Q_L}{Q_{L+}Q_G} = \frac{v_{SL}}{v_{SL} + v_{SG}} \qquad 7$$

2.2 Criteria for selecting gas-liquid experimental datasets in the literature

Not all published experimental gas-liquid flow datasets are fit to be included for analysis in this project. Two-phase flow characteristics vary widely depending on flow rates, physical properties of the two phases, and geometrical variables of the pipe (shape, equivalent diameter, inclination angle, etc.) (Tzotzi et al., 2011). A few of these parameters were used to guide selection of the appropriate experimental studies for analysis. Table 1 gives the general requirements for screening experimental datasets available in the public domain for inclusion into the data bank for this study. The ranges of operating conditions, geometry and fluid properties for selecting experimental datasets are provided in the 'Criterion' column of Table 1, together with corresponding dimensionless parameters Re, We, Fr, G/V, and Eo.

Table 1: Factors considered in selecting suitable literature experimental studies for analysis with relevant dimensionless parameters.

Group of factors	Factor	Criterion	Reasons
Pipe geometry	Pipe inclination	Horizontal (0°)	• Pipe inclination influences prevailing flow configurations. According to Spedding and Nguyen (1980), some flow regimes appeared only at a particular pipe inclination and not at others, but all the flow regimes that occurred at any angle of inclination also appeared in the horizontal flow condition. • The project is entirely on horizontal pipelines, the influence of dominant forces (inertial, viscous, and gravity) change with pipe angle of inclinations.
	Pipe internal diameter	10-100 mm	• The studies on multiphase pipe flows were conducted in closed channels with inner diameters ranging from 10

			mm to 100 mm. The multiphase flow behaviours in small diameter pipes (<10 mm) are significantly different from the conventional scales, for example, the surface tension force becomes important, and separated flow is not observed (Fukano and Kariyasaki, 1993; Yang and Shieh, 2001). Likewise, large diameter pipes (>100 mm) have different flow configurations (Kaji and Azzopardi, 2010). Ohnuki and Akimoto (2000) reported that no conventional Taylor bubble appears in large diameter pipe. • Shao et al. (2009) gave three major differences comparing flows in microchannels and macro systems. In microchannels, (i) the relative importance of surface to volume forces increases; (ii) Laminar flow is usually dominant because of small Reynolds number, and hence viscous forces dominate the inertia forces; (iii) the effects of wettability, wall roughness and flow confinement become important.
Fluid properties	Density	Air ≈1.2 kg/m^3, Water ≈1000 kg/m^3, Oil ≈800-900 kg/m^3.	• Researchers' findings support that a high-density difference between phases helps in the formation of stratified flow as compared to a low-density difference. • The gas density strongly affects the transitions within the stratified flow regime (i.e. from smooth to 2-D waves and from 2-D waves to K-H waves) (Tzotzi et al., 2011). • An increase in gas density does not change the transition to slug or plug flow, but significantly decreases the critical gas velocity for the onset interfacial waves and liquid atomization (Hoogendoorn and Buitelaar, 1961; Tzotzi et al., 2011).
	Viscosity	Air ≈0.00001 Pa s, Water ≈0.001 Pa s, Oil ≈0.007 Pa s.	• Liquid viscosity does not significantly affect the transition between flow regimes (Hoogendorn, 1959; Weisman et al., 1979). • Matsubara and Naito (2011) reported that when liquid viscosity is higher than 100 mPa s, the transition lines do not agree with previous studies.
	Surface tension	0.03-0.072 N/m	• Surface tension affects the transition between flow regimes differently. It is more distinct at low gas and liquid velocities but diminished at high gas and liquid velocities (Bageri et al., 2017).
Flow conditions	Temperature	≈25℃	• The temperature has strong effects on fluid properties (i.e. viscosity, density, surface tension), which can influence the flow momentum and subsequently the flow configuration.
	Pressure	≈1 atm	• The operating pressure affects the flow regimes by the virtue of its influence on the fluid properties (Anumbe, 2018).
Dimensionless parameters	Reynolds number (Re)	300-2300000	• It is the ratio of inertia to viscous force in a two-phase flow. A high Re value implies that the flow system is probably an inertia force dominated and turbulent. This type of flow is more likely when the viscosities of the fluids are low, and the pipe diameter and fluids velocities are high.
	Weber number (We)	0.05-200000	• This is the ratio of inertia to surface tension force in a two-phase flow. A low We value indicates the dominance of surface tension; in this flow condition, separated flow is unlikely.

Froude number (Fr)	0.01-40	• It is the ratio of inertia to gravity force in a two-phase flow. A low Fr value shows that gravity force dominance is more likely.
Gravity to viscous (G/V)	200-9000000	• It is the ratio of gravity to viscous force in a two-phase flow. A low G/V value implies a flow system dominated by viscous force, which is more likely with fluids of high viscosity.
Eötvös number (Eo)	10-2000	• This is the ratio of gravity to surface tension force in a two-phase flow. It is independent of fluid velocities. It indicates if a flow system is gravity or surface tension force dominated.

2.3 Experimental datasets extracted from literature

All the literature datasets are obtained from experimental gas-liquid flow in horizontal pipes. The literature experimental database contains 2665 records contributed from 17 different experimental set-ups. Air-fresh water flow is 85.4% of the data, which operated at an average temperature of 20℃, with the fluid properties of 1.204 and 998.3 kg/m^3 as air and water density, 0.000018205 and 0.001002 Pa s as air and water viscosity, respectively, and air-water surface tension of 0.072 N/m (Barnea et al., 1980; Chen, 1979; Kong and Kim, 2017; Mathure, 2010; Nguyen, 1975; Shoham, 1982; Spedding et al., 1989; Todkar et al., 2016; Weisman et al., 1979; Wong and Yau, 1997). Light oil and air were used as the working fluids in experimental studies (Gregory et al., 1978; Kokal, 1987; Kokal and Stanislav, 1989) and contributed 14.6% to the database. The density and viscosity of light oil used were 859.9 kg/m^3 and 0.0074 Pa s, respectively, and the surface tension of air-light oil was 0.0309 N/m.

Table 2 presents the contribution of each experimental data source to the database, with the corresponding pipe diameter. The sum of data points belonging to each flow regime and total data points contributed by each data source are also shown in Table 2.

Table 2: Contribution of experimental data sources to database and each flow regime.

Data source	Diameter (mm)	ST	SW	SL	PL	BB	AN	DB	Total
Kong and Kim (2017)	38.1	23	17	43	21	14	12	0	**130**
Weisman et al. (1979)a	51	69	56	29	43	8	44	39	**288**
Weisman et al. (1979)b	12	0	17	40	36	0	36	29	**158**
Wong and Yau (1997)	12	14	14	53	13	13	61	0	**168**
Todkar et al. (2016)	23.9	5	5	0	5	5	5	0	**25**
Spedding et al. (1989)	93.5	3	61	15	0	0	6	0	**85**
Nguyen (1975)	45.5	35	52	23	0	12	60	0	**182**
Chen (1979)	45.5	19	73	12	0	8	85	0	**197**
Kokal (1987)a; Kokal and Stanislav (1989)a	25.8	1	0	22	13	0	31	12	**79**
Kokal (1987)b; Kokal and Stanislav (1989)b	51.2	14	0	25	20	0	22	13	**94**
Kokal (1987)c; Kokal and Stanislav (1989)c	71.3	28	0	10	7	0	3	0	**48**
Shoham (1982)a	51	24	30	45	22	0	26	21	**192**
Shoham (1982)b	25	50	25	53	33	0	40	13	**214**
Gregory et al. (1978)a	25.8	0	0	62	0	0	0	0	**62**
Gregory et al. (1978)b	51.2	0	0	105	0	0	0	0	**105**
Barnea et al. (1980)	25	37	19	40	27	0	32	15	**170**
Mathure (2006)	12.7	0	0	302	118	22	26	0	**468**
	Total	**346**	**369**	**879**	**358**	**82**	**489**	**142**	**2665**

Note: ST means stratified-smooth, SW means stratified-wavy, SL means slug, PL means plug, AN means annular, BB means bubble, and DB means dispersed bubble flow.

The major difficulties in compiling these data from the experimental research works are the ambiguity in the definition and different nomenclatures adopted by various researchers to describe the flow regimes (Sharma et al., 2006). Thus, a more objective and consistent way was adopted by critically analysing the definitions given to each flow regime by a researcher and then assigning the class where the flow regime fits. For sizeable and meaningful analysis, the flow regimes with common features were grouped to form stratified-smooth (ST), stratified-wavy (SW), slug (SL), plug (PL), annular (AN), bubble (BB), and dispersed bubble (DB) flow.

In all the considered experimental works for data extraction, both bubble flow and dispersed bubble flow were not considered individually in the same experiment. It is either bubble flow being considered, or dispersed bubble flow being considered, but not both. Weisman et al. (1979)a is the only exception, where construction of a gas-liquid flow map for 51mm pipe diameter contained both bubble flow and dispersed bubble flow. Therefore, in this project, datasets for both bubble flow and dispersed bubble flow are combined and considered to be a single flow regime. These two flow regimes will be referred to as dispersed bubble (DB) flow in the rest of this paper.

2.4 The MultiFlowMet II experimental setup

As well as utilising data acquired from literature survey, this study will also include several data sets generated from an experimental study as part of the European Metrology Programme for Innovation and Research (EMPIR) project 16ENG07–MultiFlowMetII. This project focused on the minimisation of laboratory-specific effects and included an intercomparison between three leading multiphase flow laboratories (Elliott et al., 2021): TÜV SÜD National Engineering Laboratory (NEL) in the UK; DNV GL in the Netherlands; and NORCE in Norway. Across all three facilities, a 76.2 mm (3 in) internal diameter steel pipe was used and in all test points, a horizontal (0° inclination) configuration was employed. Additional experimental studies were conducted at the DNV GL facility with internal diameters of 101.6 mm (4 in) and 152.4 mm (6 in). An overview of the variations between the laboratories, and the physical parameters achieved, are presented in Table 3.

Table 3: Summary of the flow parameters and flow loop geometry for the three multiphase laboratories.

Characteristic	**NEL, low pressure**	**NEL, high pressure**	**NORCE**	**DNV GL**
Gas density (kg/m^3)	5.54-6.41	9.74-11.21	6.26-7.47	8.52-12.03
Gas viscosity (Pa.s)*10^{-5}	1.87-1.88	1.77-1.89	1.80	1.76-1.79
Water density (kg/m^3)	1023.65-1025.49	1022.79-1025.89	1031.58-1032.07	1030.87-1032.03
Oil density (kg/m^3)	814.56-829.60	813.91-818.15	823.52-824.78	825.47-828.50
Oil viscosity (Pa.s)*10^{-3}	7.26-8.26	6.95-8.51	2.4-2.7	4.8-5.2
Closed/open loop	Open	Open	Closed	Closed
Injection type	Gas into liquid	Gas into liquid	Gas into liquid	Liquid into gas

Given that the aim of this research was to assess the influence of laboratory effects on the flow measurement, the same matrix of test points was repeated at each facility, though this was separated into a lower pressure (557.28 kPa) comparison between NEL and NORCE, and a higher pressure (1013.25 kPa) comparison between NEL and DNV GL. The two test matrices showing the input liquid volumetric flow rate (Q_{liq}) and the corresponding gas volume fraction (GVF) at lower and higher pressures are presented in Table 4. The GVF value was calculated by gas volumetric flow rate against the total gas and liquid mixture volumetric flow rate local to the flow regime observation section.

Table 4: Multiphase intercomparison test matrices.

	Lower pressure							***Higher pressure***						
Q_{liq} (m^3/s)	**GVF (%)**							**GVF (%)**						
$*10^{-3}$	10	30	50	67	80	90	95	10	30	50	67	80	90	95
1.38							X							X
4.17					X	X						X	X	
8.33			X	X	X					X	X	X		
13.89		X	X	X					X	X	X			
20.83	X	X	X	X				X	X					
27.78	X													

The facilities are 3-phase systems, but the focus of this project is 2-phase flow. Therefore, the oil and water components were combined to form the liquid phase. So, the data points from the facilities can be used/employed for gas-liquid analysis. The MultiFlowMet II project primarily focused on intermittent flow, hence it generated only a few data points for stratified wavy, annular and dispersed bubble flows, with no records of the other flow regimes, as presented in Table 5.

Table 5: Data from the MultiFlowMet II project.

Diameter (mm)	**Operating pressure (kPa)**	**Stratified wavy**	**Intermittent**	**Annular**	**Dispersed bubble**	**Total**
101.6	101.32	0	326	5	2	333
152.4	101.32	1	321	3	0	325
76.2	1013.25	0	79	8	0	87
76.2	557.28	0	37	8	0	45
	Total	**1**	**763**	**24**	**2**	**790**

Note: Intermittent flow is a combination of slug flow and plug flow.

A total of 3455 datasets are available for analysis, 790 of these are from MultiFlowMet II and the remainder is extracted from experimental projects in scholarly journal articles. The major differences between the experimental datasets extracted from literature and those from the MultiFlowMet II project are as follows: most of the experiments from the literature were conducted at standard temperature and pressure conditions, and the datasets are all for pipe diameters between 10-100 mm; in MultiFlowMetII, the datasets were recently generated, with 83.8% of the data points obtained in pipe diameters greater than 100 mm at standard conditions, 42.2% out of this 83.8% were obtained with a pipe diameter of 101.6 mm, and 16.7% of the data points obtained with a pipe diameter of 76.2 mm were at elevated operating pressures (1013.25 kPa and 557.28 kPa). Therefore, the MultiFlowMet II datasets were employed to validate the constructed flow maps and check the applicability of constructed flow maps outside the range of the original datasets used for their construction.

3 RESULTS AND DISCUSSION

3.1 Construction of flow regime maps

All experimental datasets extracted from the literature are presented on the Mandhane et al. (1974) flow regime map in Figure 2a, which utilises superficial liquid velocity (v_{SL}) and superficial gas velocity (v_{SG}) as the axes. There are no newly-drawn transition boundaries in Figure 2a *Figure 2*; the Mandhane et al. (1974) transition boundaries were superimposed on data points gathered from the literature. The literature data seem to fit with the superimposed

Mandhane et al. (1974) transition boundaries in some cases, though there are notable areas that do not show agreement. The challenge in predicting transition boundaries can be easily observed in Figure 2a, particularly at the transition between SL/SW, SL/AN and the other flow regimes. As will be discussed below, only 66.6% of the data points were correctly characterised by the standard flow regime map. Therefore, there is scope for significant improvement in the predictive capabilities. Figure 2b presents a flow regime map with the coordinates of superficial liquid velocity (v_{SL}) versus superficial gas velocity (v_{SG}) with transition boundaries drawn to mark each flow regime to a distinct region. The authors note that these transition boundaries represent a non-unique classification designed to demonstrate possible improvements in the number of correctly classified test points without the utilisation of statistical methods to provide an optimised categorisation. Based on the constructed transition boundaries, 75.7% of the analysed data points were predicted correctly. In the remainder of this section, dimensionless parameter groups are used to investigate flow regime maps with more distinct boundaries.

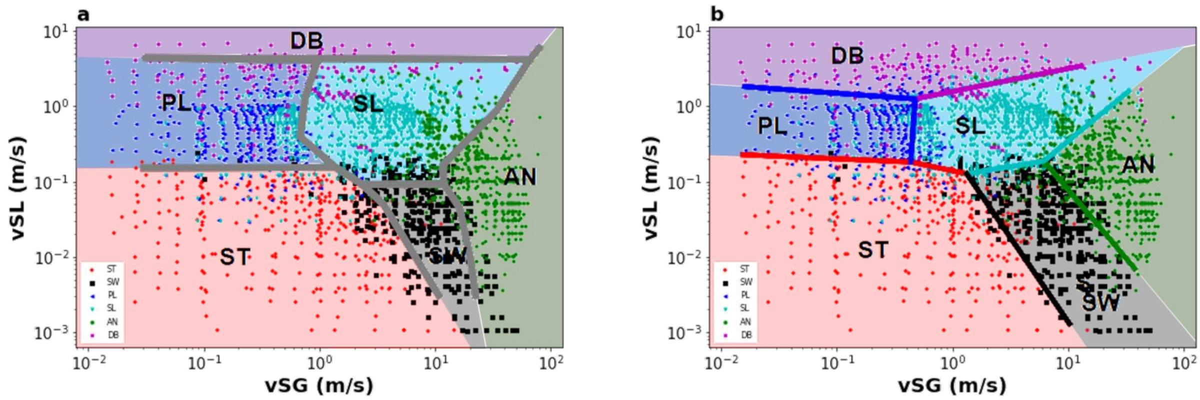

Figure 2: The flow map of superficial liquid velocity (v_{SL}) versus superficial gas velocity (v_{SG}) based on gathered literature datasets, (a) with superimposed Mandhane et al. (1974) flow map, (b) with constructed transition boundaries.

Several combinations of dimensionless parameter groups were employed for constructing flow regime maps. Some of the dimensionless parameter groups were used to normalise the chosen datasets, which were split into those from MultiFlowMet II and those extracted from published experimental works. For MultiFlowMetII, the intermittent flow was the focus, which was a combination of plug and slug flows, so the analysis of this grouping considered both plug and slug flows as intermittent flow. In the construction of flow regime maps, there are inherent challenges due to data points from different research works being assigned different names for a given flow regime, and the use of visual observation to identify flow regimes in a subjective manner. Moreover, due to dependence on the active physical mechanisms, it is unlikely that any set of two dimensionless parameters will provide a unified description of all flow regime transitions.

To address this challenge, this work considers ratios of dimensionless parameters to assess their suitability for providing a more unified flow regime map. Those combinations that neither normalised nor delineated the flow regimes will not be discussed here. Some combinations of dimensionless parameter groups give the same type of information; this is the case of We_m/Eo versus v_{SG}/v_{SL} and F_{rm} versus v_{SG}/v_{SL}, as well as We_L/Eo versus We_G/Eo and Fr_L versus Fr_G. The reason being that, by definition, both We/Eo and Fr are ratios of inertial to gravity forces, and Fr is the square root of We/Eo value (Osundare et al., 2020).

A total of seven combinations of dimensionless parameter groups was found to show good potential for constructing flow maps, however the best two flow maps are presented in Figure 3a to Figure 3b. Transition boundaries were drawn on these flow maps to enclose data points from a flow regime that could be clearly delineated into a distinct area or region on the flow map. No transition boundaries were drawn in the absence of a clear distinction between data points of two flow regimes.

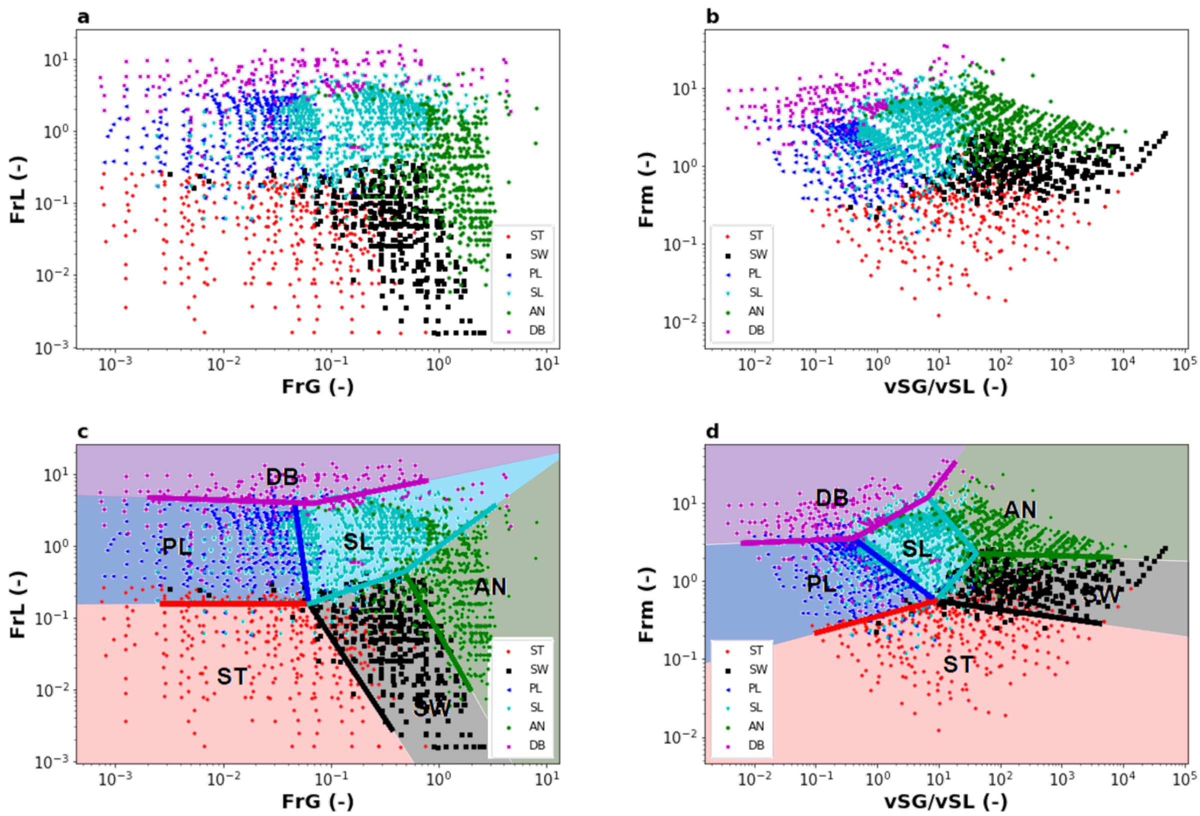

Figure 3: Constructing transition boundaries for datasets extracted from experimental works in the literature; (a) Fr_L versus Fr_G; (b) Fr_m versus v_{SG}/v_{SL} (c) Fr_L versus Fr_G with transition boundaries; (d) Fr_m versus v_{SG}/v_{SL} with transition boundaries.

All the flow regimes were normalised and delineated by the combination of Fr_L versus Fr_G, as presented in Figure 3a. Based on the data points analysed, the combination of Fr_m versus v_{SG}/v_{SL} normalised and delineated all the considered flow regimes, as presented in Figure 3b. The transition boundaries associated with the maps of Fr_L versus Fr_G and Fr_m versus v_{SG}/v_{SL} are presented in Figure 3c and Figure 3d, respectively.

3.2 Performance of different combinations of dimensionless parameter groups

The accuracy of various combinations of dimensionless parameter groups was estimated by verifying the data points from experimental works in the literature against the constructed transition boundaries. The data points are grouped into matched, nearly matched, and miss-matched. The matched data points are those that were normalised and delineated and captured within the constructed transition boundaries of a particular flow regime. The nearly matched data points are those that were delineated but not captured within the constructed transition boundaries of that particular flow regime. The miss-matched data points are those that were neither normalised nor delineated and not near to the constructed transition boundaries of a specific flow regime. Data points enclosed by the transition lines were counted as matched. Parallel lines were drawn at some distance to the transition boundaries considering those data points that were delineated but not captured within the constructed transition boundaries, and the data points inside these lines were counted as nearly-matched, and those outsides were counted missed-matched. Table 6 presents a summary of the performance of various combinations of dimensionless parameter groups. The values in Table 6 are percentages of data points of a particular flow regime that are either matched or nearly matched or miss-matched.

Table 6: Accuracy of various combinations of dimensionless parameters and Mandhane et al. (1974) flow map in predicting some flow regimes in percentage (%).

Flow regimes		**ST**	**SW**	**SL**	**PL**	**DB**	**AN**	**Average**
v_{SL} versus v_{SG} superimposed by Mandhane et al. (1974) flow map	Matched	88.7	53.1	81.7	88.5	18.8	68.5	66.6
	Nearly matched	11.3	44.7	10.7	9.8	72.3	28.2	29.5
	Miss-matched	0.0	2.2	7.6	1.7	8.9	3.3	3.9
v_{SL} versus v_{SG} with constructed transition boundaries	Matched	84.4	78.3	82.0	57.0	75.4	77.3	75.7
	Nearly matched	15.6	20.1	15.4	39.1	18.3	19.2	21.3
	Miss-matched	0.0	1.6	2.6	3.9	6.3	3.5	3.0
Re_m/Eo versus v_{SG}/v_{SL}	Matched	0.0	80.2	0.0	0.0	53.1	73.2	34.4
	Nearly matched	98.6	17.9	81.2	88.8	25.0	24.1	55.9
	Miss-matched	1.4	1.9	18.8	11.2	21.9	2.7	9.6
Re_L/Eo versus Re_G/Eo	Matched	0.0	79.9	0.0	0.0	53.1	72.8	34.3
	Nearly matched	97.7	18.2	84.9	88.8	25.4	24.3	56.6
	Miss-matched	2.3	1.9	15.1	11.2	21.4	2.9	9.1
Fr_L versus Fr_G	Matched	76.0	81.3	82.5	85.2	63.4	80.16	78.1
	Nearly matched	24.0	16.8	17.5	12.6	27.7	16.16	19.1
	Miss-matched	0.0	1.9	0.0	2.2	8.9	3.68	2.8
Fr_m versus v_{SG}/v_{SL}	Matched	81.2	82.9	79.1	82.1	64.7	81.2	78.5
	Nearly matched	18.8	15.2	20.9	12.8	26.3	15.7	18.3
	Miss-matched	0.0	1.9	0.0	5.0	8.9	3.1	3.2
G/V versus v_{SG}/v_{SL}	Matched	52.9	69.9	82.9	77.4	57.6	87.5	71.4
	Nearly matched	39.0	19.2	15.4	17.9	22.3	7.6	20.2
	Miss-matched	8.1	10.8	1.7	4.7	20.1	4.9	8.4
Ca_L versus Ca_G	Matched	78.9	84.8	0.0	68.4	0.0	81.39	52.3
	Nearly matched	9.0	13.6	100.0	30.4	89.3	16.16	43.1
	Miss-matched	12.1	1.6	0.0	1.1	10.7	2.45	4.7
Ca_m versus v_{SG}/v_{SL}	Matched	79.8	83.7	0.0	65.4	0.0	82.62	51.9
	Nearly matched	8.1	14.6	100.0	32.7	89.3	14.93	43.3
	Miss-matched	12.1	1.6	0.0	2.0	10.7	2.45	4.8

Note: ST = stratified-smooth, SW = stratified-wavy, SL = slug, PL = plug, AN = annular, and DB = dispersed bubble flow.

The v_{SL} versus v_{SG} data was demonstrated to match 66.6% of the test points when the classical Mandhane et al. (1974) flow map was applied, but this figure was increased to 75.7% when the approach outlined in this paper was applied. This increase confirms the hypothesis that there is potential to improve the classification of flow regimes by using dimensionless parameter groups, though the authors note that maps presented in this paper provide a proof-of-concept for such improvements, rather than an optimal categorisation. Moreover, the combinations of Fr_m versus v_{SG}/v_{SL} (78.5% of points matched) and Fr_m versus Fr_L (78.1% of points matched) demonstrate the potential for further increases in accuracy through the exploration of additional dimensionless parameter groups.

For the ST flow regime, the combinations Fr_mversus v_{SG}/v_{SL}, Fr_L versus Fr_G, and the v_{SL} versus v_{SG} superimposed by Mandhane et al. (1974) have flow map zero miss-matched cases. All the combinations of dimensionless parameter groups have a matched result >75% except for G/V versus v_{SG}/v_{SL} with 52.9%, as shown in Table 6. The v_{SL} versus v_{SG} superimposed by Mandhane et al. (1974) has the highest matched cases of 88.7%.

For the SW flow regime, the v_{SL} versus v_{SG} superimposed by Mandhane et al. (1974) has the least matched cases of 53%, all the combinations of dimensionless parameter groups have a matched result of >80%, with the exception of G/V versus v_{SG}/v_{SL} with 69.9%, as shown in Table 6. The miss-matched result in all the combinations of dimensionless parameter groups is 1.9%, which is lesser than 2.2% miss-matched result for the superimposed Mandhane et al. (1974) flow map except for G/V versus v_{SG}/v_{SL} with 10.8%, as shown in Table 6.

For the SL flow regime, the combinations of Fr_m versus v_{SG}/v_{SL} and Fr_L versus Fr_G have zero miss-matched cases. These combinations of dimensionless parameter groups have a >80% matched result, with the exception of Fr_m versus v_{SG}/v_{SL} with 79.1%, whereas the superimposed Mandhane et al. (1974) flow map has a matched result of 81.7% with a miss-matched result of 7.6%, as shown in Table 6. Both Re_m/Eo versus v_{SG}/v_{SL} and Re_L/Eo versus Re_G/Eo flow maps have zero matched results because no region can be marked out for the slug flow. In Ca_L versus Ca_G and Ca_m versus v_{SG}/v_{SL} flow maps, zero matched results were recorded because the bubble flow data points overlapped the slug region, but the slug flow data points were all normalised giving a miss-matched and nearly matched results of 0% and 100%, respectively.

For the PL flow regime, both Re_m/Eo versus v_{SG}/v_{SL} and Re_L/Eo versus Re_G/Eo flow maps have zero matched results. The superimposed Mandhane et al. (1974) flow map and all the other combinations of dimensionless parameter groups in exception of Ca_L versus Ca_G and Ca_m versus v_{SG}/v_{SL} flow maps recorded a >75% matched result, as presented in Table 6.

For the DB flow regime, apart from Ca_L versus Ca_G and Ca_m versus v_{SG}/v_{SL} flow maps where the DB data points formed more than one trend and no matched result could be recorded, v_{SL} versus v_{SG} with constructed transition boundaries has the highest matched result of 75.4%, but the superimposed Mandhane et al. (1974) flow map has the lowest matched result (18.8%), as presented in Table 6. The combination of Re_m/Eo versus v_{SG}/v_{SL} has the highest miss-matched result of 21.9%, as presented in Table 6. The DB flow regime has the highest miss-matched result which could be due to the DB flow data being a combination of data from two distinct flow regimes (bubble flow and disperse bubble flow).

For the AN flow regime, the matched result recorded in all the combinations of dimensionless parameter groups is better than 68.5% for the superimposed Mandhane et al. (1974) flow map. The combination of G/V versus v_{SG}/v_{SL} has the highest matched result of 87.5%, but also with the highest miss-matched result (4.9%).

3.3 Superimposing the transition boundaries on the MultiFlowMet II datasets

3.3.1 Transition boundaries superimposed on superficial liquid velocity versus superficial gas velocity

Figure 4 presents the flow regime map of the MultiFlowMet II datasets using the y-x axes of the superficial liquid velocity (v_{SL}) versus superficial gas velocity (v_{SG}) with superimposed transition boundaries.

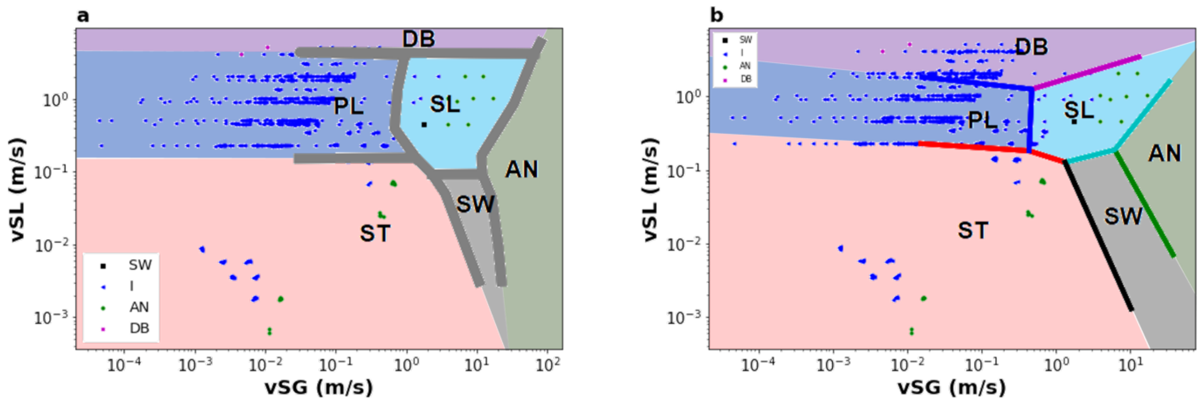

Figure 4: The flow map of superficial liquid velocity (v_{SL}) versus superficial gas velocity (v_{SG}) based on the datasets from MultiFlowMet II projects, (a) superimposed Mandhane et al. (1974) flow map, (b) with constructed transition boundaries.

Note: Intermittent flow (I) is a combination of slug flow (SL) and plug flow (PL).

The MultiFlowMet II data points are presented with the Mandhane et al. (1974) and constructed flow maps in Figure 4a and 4b, respectively. While the classical map correctly characterises 95.5% of the test points, only 67.9% of points are correctly identified by the constructed flow regime map. In particular, a significant number of PL data points are incorrectly categorised as DB, though the two dispersed bubble flow points are more accurately categorised. This disparity is likely explained by the fact that 321 of the 763 intermittent test points were conducted using a pipe diameter of 152.4 mm, which is beyond the 10-100 mm range used to define the flow boundaries, which was not the case for Mandhane et al. (1974). This distinction raises an important point regarding the scalability of flow regime maps, as will be explored in future work.

3.3.2 Dimensionless parameter group transition boundaries

As can be concluded from Section 3.3.1, there is clear scope to improve the accuracy of the newly constructed flow regime maps through the application of alternative dimensionless parameter groups. The combinations listed in Table 6 were again utilised for the MultiFlowMet II data. From the seven combinations of dimensionless parameter groups analysed, FrL versus Fr_G and Frm versus v_{SG}/v_{SL} flow maps are presented in Figure 5; these results represent the most viable candidates for delineating the new data set.

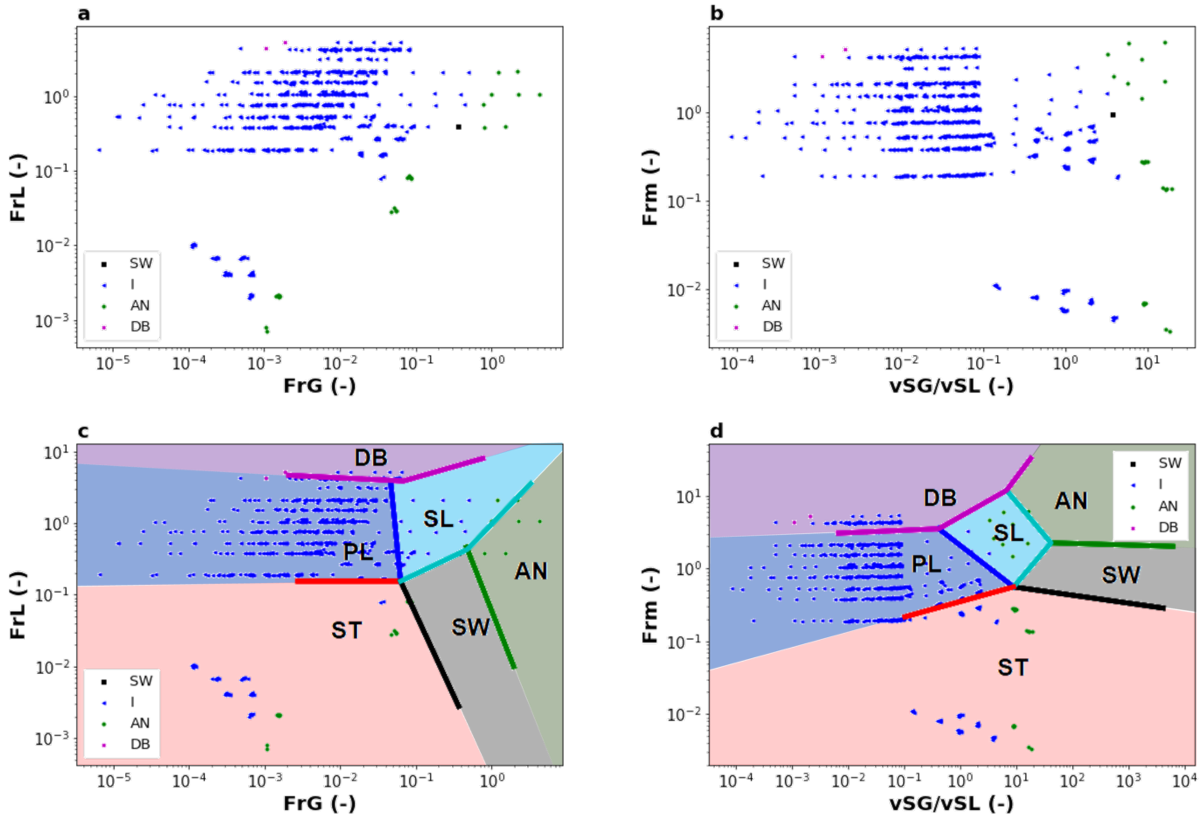

Figure 5: Superimposing the transition boundaries of datasets extracted from experimental works in the literature on the datasets from MultiFlowMet II projects; (a) Fr_L versus Fr_G; (b) Fr_m versus v_{SG}/v_{SL}. (c) Fr_L versus Fr_G with transition boundaries; (d) Fr_m versus v_{SG}/v_{SL} with transition boundaries.

The Fr_L versus Fr_G flow regime map, presented in Figure 5c, correctly matched 92.7% of intermittent flow test points, whereas a figure of 88.9% was achieved for the Fr_m versus v_{SG}/v_{SL} map. Thus, this new choice of parameter groups represents a clear improvement from the attempts made using only the superficial velocities. This is likely to be as a result of the explicit inclusion of the pipe diameter in the definition of Froude number (Equation 2). However, the slight underperfromance in comparison with the traditional flow regime map suggests that further improvements could be made by including physical knowledge of the flow regime transitions in constructing the boundaries.

The incorrect prediction of annular test points is largely consistent between the v_{SG} versus v_{SL} maps (traditional and constructed) and the Fr_m versus v_{SG}/v_{SL} map, though this is somewhat improved by the comparison of Froude numbers, which correctly identifies 25% of the points. Of the dimensionless parameter groups considered, no significant improvement on this fraction was achieved, which may be explained by the impact of variations in pipe diameter on the transition from stratified flow (Emamzadeh and Issa, 2013).

3.4 Discussion of results

The combinations of dimensionless parameter groups employed for constructing flow regime maps in this project are:

1. The ratio of mixture Reynolds number to Eötvös number (Re_m/Eo) versus the ratio gas superficial velocity to liquid superficial velocity (v_{SG}/v_{SL}).

2. The ratio of liquid Reynolds number to Eötvös number (Re_L/Eo) versus gas Reynolds number to Eötvös number (Re_G/Eo).
3. The mixture Froude number (Fr_m) versus the ratio gas superficial velocity to liquid superficial velocity (v_{SG}/v_{SL}).
4. The liquid Froude number (Fr_L) versus gas Froude number (Fr_G).
5. The liquid capillary number (Ca_L) versus gas capillary number (Ca_G).
6. The mixture capillary number (Ca_m) versus the ratio gas superficial velocity to liquid superficial velocity (v_{SG}/v_{SL}).
7. The ratio of gravity force to viscous force (G/V) versus the ratio gas superficial velocity to liquid superficial velocity (v_{SG}/v_{SL}).

Some combinations of dimensionless parameter groups such as Fr_L versus Fr_G, and Fr_m versus v_{SG}/v_{SL} were successful in normalising and delineating the MultiFlowMet II intermittent data points and were able to match the superimposed transition boundaries by 92.7% and 88.9%, respectively, as presented in Figure 5c and 5d. This was in spite of a wide range of pipe diameters (76.2-152.4 mm) and 3 different operating pressures (101.32, 557.28 and 1013.25 kPa.) used in MultiFlowMetII. These combinations of dimensionless parameter groups have good potential to normalise and delineate intermittent flow.

Clerc (2000) and De Lorenzo et al. (2017) stated that the mixture-component based on homogeneous equilibrium model is well-designed to simulate/predict the dispersed bubble flow, but cannot reproduce mechanical or thermodynamic non-equilibrium flow, such as annular flows. This is consistent with the results obtained when superimposing the transition boundaries from experimental works in the literature on MultiFlowMet II datasets. Only 4.2% of MultiFlowMet II annular data points fit in the annular region of the superimposed transition boundaries for Fr_m versus v_{SG}/v_{SL}, but the combinations of Fr_L versus Fr_G has 25%, as shown in Figure 5d and Figure 5c. Yet, the superimposed Mandhane et al. (1974) flow map has zero matched results for the MultiFlowMet II annular data points.

In all flow maps constructed and analysed using the MultiFlowMet II intermittent data points, 2.4% of these data points were miss-matched. These miss-matched data points appeared to have a separate trend from the rest of the data points. All the data points in this category were found to be from the same source, the MultiFlowMet II experimental set-up with a pipe diameter of 76.2 mm and an operating pressure of 557.28 kPa. The annular flow data points in the same region were also miss-matched and from the same MultiFlowMet II experimental set-up. Once more, the disparity of the pressure—557.28 kPa for these test points in comparison with the value of 1 atm (101.325 kPa) for the flow map definition—has a clear impact on their accuracy. Future developments in this area should account for such variations to create a more scalable characterisation.

The flow regime maps for We_m/Eo versus v_{SG}/v_{SL} and Fr_m versus v_{SG}/v_{SL} gave the same type of information, except for the magnitude of values on the vertical axis, as Fr^2 equals We/Eo. Similar observations apply to the flow maps of We_L/Eo versus We_G/Eo and Fr_L versus Fr_G although in this case the magnitude of values differs for both abscissa and ordinate in the flow maps of We_L/Eo versus We_G/Eo and Fr_L versus Fr_G. Therefore, data points with the same flow characteristics would be normalised and delineated into a similar flow regime when axes of the flow map capture the same ratio of forces influencing a flow system.

4 CONCLUSIONS

In the quest to construct more generalised flow regime maps for gas-liquid flow in horizontal pipelines, datasets were obtained from the MultiFlowMet II project and relevant experimental studies in the literature, to create a robust databank for analysis. Dimensional analysis was performed on the gas-liquid flow in a horizontal pipe to obtain relevant dimensionless parameter groups, combining forces acting on the flow system.

Based on the analysed datasets, the combinations of dimensionless parameter groups formulated using mixture-component is less effective than those developed using the phase-component in normalising and delineating annular flow. This is because combinations based on mixture-components are well-designed to simulate mechanical or thermodynamic equilibrium flows, such as dispersed bubble flow, but cannot reproduce mechanical or thermodynamic non-equilibrium flows like annular flow.

Based on the analysed datasets, the combinations of the Fr_m versus v_{SG}/v_{SL} and Fr_L versus Fr_G dimensionless parameter groups show good potential in normalising and delineating the MultiFlowMet II intermittent data points. Therefore, the feasibility study presented in this work provides important evidence for improving the prediction of multiphase flow regimes in horizontal pipes through the use of dimensionless parameter groups. The development of this work will focus on the introduction of a physics-informed machine learning approach to produce optimised flow regime maps that incorporate physical knowledge of individual flow regime transitions.

ACKNOWLEDGMENTS

Olusegun Samson Osundare would like to thank the Petroleum Technology Development Fund (PTDF) for sponsoring his PhD studies. The authors are grateful for the data access granted by European Metrology Programme for Innovation and Research (EMPIR) project ‘Multiphase flow reference metrology’ (16ENG07 –MultiFlowMetII), co-funded by the European Union's Horizon 2020 research and innovation programme and the EMPIR participating states.

CONFLICTS OF INTEREST

The authors declare no conflict of interest.

NOMENCLATURE

Symbol/ Abbreviation	Unit	Interpretation	Flow regime Abbreviation	Interpretation
A	m^2	Pipe cross-sectional area	**AN**	Annular flow
d	m	Diameter	**BB**	Bubble flow
E	J	Kinetic Energy	**D**	Dispersed
Eo	-	Eötvös number	**DB**	Dispersed bubble flow
Fr	-	Froude number	**DBF**	Dispersed bubble and froth
G	$kg/m^2\ s$	Mass flux	**DL**	Droplet
g	m/s^2	Acceleration due to gravity	**EB**	Elongated bubble
G/V	-	Ratio of the gravitational force to viscous force	**EDB**	Elongated bubble and dispersed bubbles
GVF	-	Gas volume fraction	**I**	Intermittent flow
M	kg/s	Mass flow rate	**IW**	Inertial wave
N/A	-	Not applicable	**PL**	Plug flow

NR	-	Not reported	**RiW**	Ripple wave
Q	m^3/s	Volumetric flow rate	**RW**	Roll wave
Re	-	Reynolds number	**S**	Smooth
Re/Eo	-	Ratio of Reynolds number to Eötvös number	**SL**	Slug flow
$\mathbf{v_m}$	m/s	Mixture velocity	**SLF**	Slug and froth
$\mathbf{v_{SG}}$	m/s	Superficial gas velocity	**ST**	Stratified smooth flow
$\mathbf{v_{SG}/v_{SL}}$	-	Ratio of superficial gas velocity to superficial liquid velocity	**SW**	Stratified wavy flow
$\mathbf{v_{SL}}$	m/s	Superficial liquid velocity		
We	-	Weber number	**Subscript**	
We/Eo	-	Ratio of Weber number to Eötvös number	**G**	Gas phase
x	-	Quality	**L**	Liquid phase
$\boldsymbol{\alpha}$	-	Wettability	**m**	Mixture
λ	-	Baker correction factor	**O**	Oil phase
ϕ	-	Baker correction factor	**T**	Total
$\boldsymbol{\Theta}$	°	Inclination angle		
$\boldsymbol{\mu}$	mPa s	Oil viscosity		
$\boldsymbol{\rho}$	kg/m^3	Density		
$\boldsymbol{\sigma}$	N/m	Surface tension		
$\boldsymbol{\varepsilon}$	-	Void fraction		

REFERENCES

Al-Sheikh, J.N., Saunders, D.E., Brodkey, R.S., 1970. Prediction of flow patterns in horizontal two-phase pipe flow. Can. J. Chem. Eng. 48, 21–29. https://doi.org/10.1002/cjce.5450480105

Alves, G.E., 1954. Cocurrent liquid-gas flow in a pipeline contractor. Chem. Eng. Prog. 50, 449–456.

Amaya-Gomez, R., López, J., Pineda, H., Urbano-Caguasango, D., Pinilla, J., Ratkovich, N., Muñoz, F., 2019. Probabilistic approach of a flow pattern map for horizontal, vertical, and inclined pipes. Oil Gas Sci. Technol. 74. https://doi.org/10.2516/ogst/2019034

Anumbe, N.C., 2018. Experimental Investigation of Two-Phase (Gas/Liquid) Flow in Intermediate Sized, Horizontal and Inclined Pipes (PhD Thesis). University of South Carolina, Columbia, USA.

Baba, Archibong-Eso, Aliyu, Ribeiro, Lao, Yeung, 2019. Slug Translational Velocity for Highly Viscous Oil and Gas Flows in Horizontal Pipes. Fluids 4, 170. https://doi.org/10.3390/fluids4030170

Bageri, A.S., Gajbhiye, R., Abdulraheem, A., 2017. Evaluating the Effect of Surface Tension on Two-Phase Flow in Horizontal Pipes, in: SPE Kingdom of Saudi Arabia Annual Technical Symposium and Exhibition. Society of Petroleum Engineers, Dammam, Saudi Arabia, pp. 2268–2279. https://doi.org/10.2118/188009-MS

Bai, Y., Bai, Q., 2019. Hydraulics, in: Subsea Engineering Handbook. Elsevier, pp. 315–361. https://doi.org/10.1016/B978-0-12-812622-6.00013-0

Baker, O., 1954. Simultaneous flow of oil and gas. Oil Gas J. 53, 183–195.

Barnea, D., Shoham, O., Taitel, Y., Dukler, a. E., 1980. Flow pattern transition for gas-liquid flow in horizontal and inclined pipes. Comparison of experimental data with theory. Int.

J. Multiph. Flow 6, 217–225. https://doi.org/10.1016/0301-9322(80)90012-9

Bergelin, O., Gazley, C.J., 1949. Co-Current Gas-Liquid Flow in Horizontal Tubes. Proc. Heat Transf. Fluid Mech. Inst. 29, 5–18.

Brennen, C.E., 2005. Fundamentals of Multiphase Flow. Cambridge University Press, Cambridge, UK.

Chen, J.J.J., 1979. Two-phase gas-liquid flow with particular emphasis on holdup measurements and predictions (PhD Thesis). University of Auckland, Auckland, New Zealand.

Cheng, L., Ribatski, G., Thome, J.R., 2008. Two-phase flow patterns and flow-pattern maps: Fundamentals and applications. Appl. Mech. Rev. 61, 0508021–05080228. https://doi.org/10.1115/1.2955990

Clerc, S., 2000. Numerical Simulation of the Homogeneous Equilibrium Model for Two-Phase Flows. J. Comput. Phys. 161, 354–375. https://doi.org/10.1006/jcph.2000.6515

Coleman, J.W., Garimella, S., 1999. Characterization of two-phase flow patterns in small diameter round and rectangular tubes. Int. J. Heat Mass Transf. 42, 2869–2881. https://doi.org/10.1016/S0017-9310(98)00362-7

De Lorenzo, M., Lafon, P., Di Matteo, M., Pelanti, M., Seynhaeve, J.M., Bartosiewicz, Y., 2017. Homogeneous two-phase flow models and accurate steam-water table look-up method for fast transient simulations. Int. J. Multiph. Flow 95, 199–219. https://doi.org/10.1016/j.ijmultiphaseflow.2017.06.001

Eaton, B.A., Knowles, C.R., Silberbrg, I.H., 1967. The Prediction of Flow Patterns, Liquid Holdup and Pressure Losses Occurring During Continuous Two-Phase Flow In Horizontal Pipelines. J. Pet. Technol. 19, 815–828. https://doi.org/10.2118/1525-pa

Elliott, A.J., Falcone, G., Putten, D. Van, Leonard, T., Haukalid, K., Pinguet, B., 2021. Investigating reproducibility in multiphase flow metrology : Results from an intercomparison of laboratories. Flow Meas. Instrum. 79, 101951. https://doi.org/10.1016/j.flowmeasinst.2021.101951

Emamzadeh, M., Issa, R.I., 2013. One-dimensional modelfor numerical simulation of annular flow in horizontal and vertical pipes. Multiph. Sci. Technol. 25, 25–56. https://doi.org/10.1615/MultScienTechn.v25.i1.20

Farokhpoor, R., Liu, L., Langsholt, M., Hald, K., Amundsen, J., Lawrence, C., 2020. Dimensional analysis and scaling in two-phase gas–liquid stratified pipe flow–Methodology evaluation. Int. J. Multiph. Flow 122, 103139. https://doi.org/10.1016/j.ijmultiphaseflow.2019.103139

França, F., Lahey, R.T., 1992. The use of drift-flux techniques for the analysis of horizontal two-phase flows. Int. J. Multiph. Flow 18, 787–801. https://doi.org/10.1016/0301-9322(92)90059-P

Fukano, T., Kariyasaki, A., 1993. Characteristics of gas-liquid two-phase flow in a capillary tube. Nucl. Eng. Des. 141, 59–68. https://doi.org/10.1016/0029-5493(93)90092-N

Govier, G.W., Omer, M.M., 1962. The horizontal pipeline flow of air-water mixtures. Can. J. Chem. Eng. 40, 93–104. https://doi.org/10.1002/cjce.5450400303

Gregory, G.A., Nicholson, M.K., Aziz, K., 1978. Correlation of the liquid volume fraction in the slug for horizontal gas-liquid slug flow. Int. J. Multiph. Flow 4, 33–39. https://doi.org/10.1016/0301-9322(78)90023-X

Hoogendoorn, C.J., Buitelaar, A.A., 1961. The effect of gas density and gradual vaporization on gas-liquid flow in horizontal pipes. Chem. Eng. Sci. 16, 208–221. https://doi.org/10.1016/0009-2509(61)80032-8

Hoogendorn, C.J., 1959. Gas-liquid flow in horizontal pipes. Chem. Eng. Sci. 9, 205–217. https://doi.org/10.1016/0009-2509(59)85003-X

Humami, F., Dinaryanto, O., Hudaya, A.Z., Widyatama, A., Indarto, Deendarlianto, 2018. Experimental study on the characteristics of flow pattern transitions of air-water two-phase flow in a horizontal pipe, in: AIP Conference Proceedings. https://doi.org/10.1063/1.5049977

Jayawardena, S.S., Balakotaiah, V., Witte, L.C., 1997. Flow pattern transition maps for microgravity two-phase flows. AIChE J. 43, 1637–1640. https://doi.org/10.1002/aic.690430627

Johnson, H.A., Abou-Sabe, A.H., 1952. Heat transfer and pressure drop for turbulent flow of air-water mixture in a horizontal pipe. Trans. ASME 74, 977–987.

Kaji, R., Azzopardi, B.J., 2010. The effect of pipe diameter on the structure of gas/liquid flow in vertical pipes. Int. J. Multiph. Flow 36, 303–313. https://doi.org/10.1016/j.ijmultiphaseflow.2009.11.010

Kokal, S.L., 1987. An experimental study of two-phase flow in inclined pipes (PhD Thesis). University of Calgary. https://doi.org/10.11575/PRISM/14066

Kokal, S.L., Stanislav, J.F., 1989. An experimental study of two-phase flow in slightly inclined pipes-I. Flow patterns. Chem. Eng. Sci. 44, 665–679. https://doi.org/10.1016/0009-2509(89)85042-0

Kong, R., Kim, S., 2017. Characterization of horizontal air-water two-phase flow. Nucl. Eng. Des. 312, 266–276. https://doi.org/10.1016/j.nucengdes.2016.06.016

Kosterin, S., 1949. An investigation of the influence of the diameter and inclination of a tube on the hydraulic resistance and flow structure of gas-liquid mixtures. Izvestya Akad. Nauk USSR Otd. Tekhnicheskikh Nauk 12, 1824–1830.

Lin, P.Y., Hanratty, T.J., 1987. Effect of pipe diameter on flow patterns for air-water flow in horizontal pipes. Int. J. Multiph. Flow 13, 549–563.

Lips, S., Meyer, J.P., 2011. Two-phase flow in inclined tubes with specific reference to condensation: A review. Int. J. Multiph. Flow 37, 845–859. https://doi.org/10.1016/j.ijmultiphaseflow.2011.04.005

Mandhane, J.M., Gregory, G.A., Aziz, K., 1974. A flow pattern map for gas-liquid flow in horizontal pipes. Int. J. Multiph. Flow 1, 537–553. https://doi.org/10.1016/0301-9322(74)90006-8

Mathure, N., 2010. Study of Flow Patterns and Void Fraction in Horizontal Two-Phase Flow (MSc Thesis). Oklahoma State University, Stillwater, Oklahoma, USA.

Matsubara, H., Naito, K., 2011. Effect of liquid viscosity on flow patterns of gas-liquid two-phase flow in a horizontal pipe. Int. J. Multiph. Flow 37, 1277–1281. https://doi.org/10.1016/j.ijmultiphaseflow.2011.08.001

Nguyen, V.T., 1975. Two-phase, gas-liquid concurrent flow: an investigation of holdup, pressure drop and flow pattern in a pipe at various inclinations (PhD Thesis). The University of Auckland, Auckland, New Zealand.

Ohnuki, A., Akimoto, H., 2000. Experimental study on transition of flow pattern and phase distribution in upward air-water two-phase flow along a large vertical pipe. Int. J. Multiph. Flow 26, 367–386. https://doi.org/10.1016/S0301-9322(99)00024-5

Osundare, O.S., Falcone, G., Lao, L., Elliott, A., 2020. Liquid-Liquid Flow Pattern Prediction Using Relevant Dimensionless Parameter Groups. Energies 13, 4355. https://doi.org/10.3390/en13174355

Saha, S.K., 2015. Microchannel Phase Change Transport Phenomena. Butterworth-Heinemann publications.

Shao, N., Gavriilidis, A., Angeli, P., 2009. Flow regimes for adiabatic gas-liquid flow in microchannels. Chem. Eng. Sci. 64, 2749–2761. https://doi.org/10.1016/j.ces.2009.01.067

Sharma, H., Das, G., Samanta, A.N., 2006. ANN-based prediction of two-phase gas- liquid flow patterns in a circular conduit. AIChE J. 52, 3018–3028. https://doi.org/10.1002/aic.10922

Shi, J., Lao, L., Yeung, H., 2017. Water-lubricated transport of high-viscosity oil in horizontal pipes: The water holdup and pressure gradient. Int. J. Multiph. Flow 96, 70–85. https://doi.org/10.1016/j.ijmultiphaseflow.2017.07.005

Shi, J., Yeung, H., 2017. Characterization of liquid-liquid flows in horizontal pipes. AIChE J. 63, 1132–1143. https://doi.org/10.1002/aic.15452

Shoham, O., 2005. Mechanistic Modeling of gas liquid two phase flow in pipes. The Society of Petroleum Engineers (SPE), Tulsa.

Shoham, O., 1982. Flow Pattern Transition and Characterization in Gas-Liquid Two-Phase Flow in Inclined Pipes (PhD Thesis). Tel-Aviv University, Tel Aviv, Isreal.

Simpson, H.C., Rooney, D.H., Grattan, E., Al-Samarrae, F.A.A., 1977. Two-phase flow studies in large diameter horizontal tubes., in: European Two-Phase Flow Group Meeting.

Spedding, P.L., Chen, J.J.J., 1981. A simplified method of determining flow pattern transition of two-phase flow in a horizontal pipe. Int. J. Multiph. Flow 7, 729–731. https://doi.org/10.1016/0301-9322(81)90042-2

Spedding, P.L., Chen, J.J.J., 1980. Two Phase Flow Pressure Loss Prediction, in: National Conference Publication - Institution of Engineers, Australia. Brisbane, pp. 420–423.

Spedding, P.L., Hand, N.P., Spence, D.R., 1989. Data on horizontal, co-current, two phase gas-liquid flows.

Spedding, P.L., Nguyen, V.T., 1980. Regime maps for air water two phase flow. Chem. Eng. Sci. 35, 779–793. https://doi.org/10.1016/0009-2509(80)85062-7

Todkar, S.R., Kapale, U.C., Anil, T.R., Chapgaon, A.N., 2016. An Experimental Study on

Two Phase (Air-Water) Flow Characteristics in a Horizontal Pipe at Atmospheric Conditions. Int. J. Eng. Res. Technol. 5, 687–692.

Troniewski, L., Ulbrich, R., 1984. The analysis of flow regime maps of two-phase gas-liquid flow in pipes. Chem. Eng. Sci. 39, 1213–1224. https://doi.org/10.1016/0009-2509(84)85082-4

Tzotzi, C., Bontozoglou, V., Andritsos, N., Vlachogiannis, M., 2011. Effect of fluid properties on flow patterns in two-phase gas-liquid flow in horizontal and downward pipes. Ind. Eng. Chem. Res. 50, 645–655. https://doi.org/10.1021/ie100239v

Vásquez, F., Stanko, M., Vásquez, A., De Andrade, J., Asuaje, M., 2012. Air-water: Two phase flow behavior in a horizontal pipe using computational fluids dynamics (CFD). WIT Trans. Eng. Sci. 74, 381–392. https://doi.org/10.2495/AFM120341

Weisman, J., Duncan, D., Gibson, J., Crawford, T., 1979. Effects of Fluid Properties and Pipe Diameter on Two- Phase Flow Patterns in Horizontal Lines. Int. J. Multiph. Flow 5, 437–462. https://doi.org/10.1016/0301-9322(79)90031-4

White, P.D., Huntington, R.L., 1955. Horizontal Co-Current Two-Phase Flow of Fluids in Pipe Lines. Pet. Eng. 27, D40–D45.

Wong, T.N., Yau, Y.K., 1997. Flow patterns in two-phase air-water flow. Int. Commun. Heat Mass Transf. 24. https://doi.org/https://doi.org/10.1016/S0735-1933(96)00110-8

Xiao, J.J., Shoham, O., Brill, J.P., 1990. Comprehensive mechanistic model for two-phase flow in pipelines. Proc. - SPE Annu. Tech. Conf. Exhib. Pi, 167–180.

Yang, C.-Y., Shieh, C.-C., 2001. Flow pattern of air–water and two-phase R-134a in small circular tubes. Int. J. Multiph. Flow 27, 1163–1177. https://doi.org/10.1016/S0301-9322(00)00070-7

Zhang, H.Q., Wang, Q., Sarica, C., Brill, J.P., 2004. Unified model for gas-liquid pipe flow via slug dynamics - Part 1: Model development. SPE Repr. Ser. 125, 44–51. https://doi.org/10.1115/1.1615246

Zhao, L., Rezkallah, K.S., 1993. Gas-liquid flow patterns at microgravity conditions. Int. J. Multiph. Flow 19, 751–763. https://doi.org/10.1016/0301-9322(93)90041-R

5 APPENDIX A

5.1 Development of flow regime maps for gas-liquid flow in horizontal pipelines

Different research groups have employed various combinations of coordinates for presenting flow regime maps in a 2D graph. Table 7 shows the chronological developments of flow regime maps over the years for gas-liquid flow in horizontal pipelines.

Table 7: Development of flow regime maps for gas-liquid in a horizontal pipeline.

Author	Pipe size (mm)	Fluids	Coordinates	Identified flow patterns
Bergelin and Gazley (1949)	25.4	Air-water	Gas mass flow rate (M_G) versus liquid mass flow rate (M_L)	NR
Kosterin (1949)	25.4, 50.8,	Air-water	Mixture velocity (v_m) versus input gas volume fraction (v_{SG}/v_m)	NR

	76.2, 101.6			
Johnson and Abou-Sabe (1952)	22.1	Air-water	Gas mass flow rate (M_G) versus liquid mass flow rate (M_L)	NR
Alves (1954)	26.6	Air-water; Air-oil	Superficial gas velocity (v_{SG}) versus superficial liquid velocity (v_{SL})	BB, SL, PL, ST, SW, AN, spray
Baker (1954)	25.4-101.6	Air-water; NG-oil	G_G/λ *and* $G_L\lambda\phi/G_G$ (λ, ϕ are parameters which account for different gas and liquid properties)	ST, SW, PL, SL, AN, BB or froth and D
White and Huntington (1955)	25.4; 38.1; 50.8.	Air-water; Air-oil; NG-oil	Liquid mass flux (G_L) versus gas mass flux (G_G)	NR
Hoogendorn (1959)	24-140^S; 50^r	Air-water	Mixture velocity (v_m) versus input gas volume fraction (v_{SG}/v_m)	ST, SW, PL, SL, mist-AN, and froth
Govier and Omer (1962)	26.1	Air-water	Liquid mass flux (G_L) versus gas mass flux (G_G)	ST, SW, PL, SL, BB, AN
Eaton et al. (1967)	50.8; 101.6.	NG-water; NG-crude oil; NG-distillate	Two-phase Reynolds number (Re_{tp}) versus two-phase Weber number (We_{tp})	NR
Al-Sheikh et al. (1970)	18.7-154.1	Gas-liquid	10 coordinates derived from the authors 9 correlations.	BB, PL, ST, SW, SL, AN, spray
Mandhane et al. (1974)	12.7-165.1	Gas-liquid	Superficial liquid velocity (v_{SL}) versus superficial gas velocity (v_{SG})	BB, ST, SW, SL, AN-mist, DB
Simpson et al. (1977)	127; 216	Air-water	Superficial liquid velocity (v_{SL}) versus superficial gas velocity (v_{SG})	N/A
Weisman et al. (1979)	12; 25; 51	Air-water; Air-glycerol	Gas mass flux (G_G) versus liquid mass flux (G_L)	PL, BB, ST, SW, SL, AN, D
Spedding and Nguyen (1980)	45.5	Air-water	Froude number ($v_m/\sqrt{g\,d}$) versus volumetric flow ratio (Q_L/Q_G)	13 distinguishable flow patterns lumped to 4 types of flow: stratified, bubble & slug, droplets, mixed
Spedding and Chen (1981)	13-50	Gas-liquid	Superficial liquid velocity (v_{SL}) versus superficial gas velocity (v_{SG})	AN, PL or long BB, ST+ripple, SL, ST, ST+roll wave
Lin and Hanratty (1987)	25.4; 95.3	Air-water	Superficial liquid velocity (v_{SL}) versus superficial gas velocity (v_{SG})	ST, SW, SL, AN, pseudo-SL
Kokal and Stanislav (1989); Kokal (1987)	25.8; 51.2; 713	Air-light oil	Superficial liquid velocity (v_{SL}) versus superficial gas velocity (v_{SG})	ST, SW, AW, EB, EDB, SL, SLF, DB, DBF
Xiao et al. (1990)	50	Air-water	Superficial liquid velocity (v_{SL}) versus superficial gas velocity (v_{SG})	ST, SW, AN, DB, I
Wong and Yau (1997)	12	Air-water	Superficial liquid velocity (v_{SL}) versus superficial gas velocity (v_{SG})	16 distinct flow patterns lumped to 4 flow types: i. ST: S, IW, RiW, RW

				ii. I: PL, SL, PL-SL, pseudo-SL iii. DB iv. MF: RW+DL, RW+DL+AN, RW+AN, pseudo-SL+AN, pseudo-SL+thin AN, SL-AN, DB+SL
Jayawardena et al. (1997)	9.5-40	Gas-liquid		BB, SL, AN
Tzotzi et al. (2011)	24	He-water; Air-water; CO_2-water; Air-aqueous butanol	-Superficial liquid velocity (v_{SL}) versus superficial gas velocity (v_{SG}) - Superficial liquid velocity (v_{SL}) versus superficial gas velocity multiply by the square root of ratio of liquid density to gas density (v_{SG} *(ρ_L/ρ_G))	ST, SL, SL-froth, AN
Kong and Kim (2017)	38.1	Air-water	Superficial liquid velocity (v_{SL}) versus superficial gas velocity (v_{SG})	BB, PL, SL, ST, SW and AN

Note: others means used data from others studies; [s] and [r] indicate smooth and rough pipe, respectively; NG means Natural-gas, NR means not reported; ST: stratified; SW: stratified wavy; AN: annular; EB: elongated bubble; EDB: elongated bubble and dispersed bubbles; SL: slug; SLF: slug and froth; DB: dispersed bubble; DBF: dispersed bubble and froth; BB: bubble; D: dispersed; PL: plug; I: intermittent, IW: inertial wave; RiW: ripple wave; RW: roll wave; DL: droplet; S: smooth.

Based on Table 7, the superficial liquid velocity (v_{SL}) versus superficial gas velocity (v_{SG}) is the most frequently used for constructing flow maps in recent times. This may be due to the assumption that transition curves are least sensitive to changes in pipe diameter and fluid properties when superficial liquid velocity (v_{SL}) and superficial gas velocity (v_{SG}) are used as coordinates (Lin and Hanratty, 1987).

The choice of coordinate systems (ordinate and abscissa) used for constructing a flow pattern map is divided into three groups, according to Cheng et al. (2008); Troniewski and Ulbrich (1984):

1. Phase velocities or fluxes (group I): The parameters include gas and liquid superficial velocities (v_{SG}, v_{SL}), gas and liquid mass flow rates (M_G, M_L), gas and liquid mass fluxes (G_G, G_L). They are convenient to employ but cannot create universal flow pattern maps for different two-phase combinations.
2. Quantities that refer to the homogeneous model of a two-phase flow (group II): They are the transformation of parameters from group I, which include total velocity (v_T), total mass flux (G_T), Froude number based on total velocity (Fr_T), void fraction (ε), and quality (x). Valid only for some flow patterns.
3. Parameters comprising the physical properties of the phases (group III): These include gas and liquid Reynolds numbers (Re_G, Re_L), Baker correction factors (λ, ϕ), gas and liquid kinetic energies (E_G, E_L). This group has the best potential to provide universal flow regime maps.